author's personal copy

DOI: 10.1002/adem.((please add manuscript number))

Plasticity mechanisms in sub-micron Al fiber investigated by in situ TEM **

By *F.Mompiou*, and *M. Legros**

[*] *F. Mompiou Corresponding-Author, M. Legros*
CEMES-CNRS, 29 rue Marvig
31055 Toulouse cedex 4
E-mail: mompiou@cemes.fr, legros@cemes.fr

[**] *The authors acknowledge the support of the ESTEEM project for funding. Supporting Information is available online from Wiley InterScience or from the author.*

Sub-micron Al fibers have been tested mechanically in-situ in a transmission electron microscope. Their plastic behaviour appears to be strongly sensitive to their initial dislocation content. We report here observations on fibers that were obtained by a chemical etching of a eutectic alloy where isolated and stable sources operate. The strength of sources in fibers of different size has been directly measured. We show that the increase of the yield stress with decreasing fiber size can be directly attributed to the increase of the source strength.

While most of the micro-mechanical tests performed in the last 10 years seem to conclude on a size effect in plasticity, the nature of the elementary deformation mechanisms in small scale single crystals is still the subject of debate [1],[2]. Contrary to defect-free whiskers which fail in a brittle manner, sometimes close to the theoretical stress [3],[4], sub-micron metallic single crystals exhibit a ductile behavior. These single crystals are usually carved out by FIB with a pillar shape and tested by flat-punch nano-indentation [5]. In the plastic regime they exhibit an unusual behavior consisting in strain bursts and strong hardening [6] [7] [8] [9].

Despite their crystalline structure, their yield stress obeys a universal power law $\sigma = \frac{k}{d^n}$ with

author's personal copy

n ranging from 0.6 to 1 [1]. This exponent n has been found to depend on the critical temperature in bcc metals [10]. In several recent studies, Bei et al. have shown that this behavior is strongly related to an initial microstructure containing enough dislocations to sustain plastic deformation [11], [12] [13]. In the extreme case where no dislocations are present (whisker case), they were able to suppress the size effect [14]. Mainly two dislocation-based theories have been recently proposed to account for this power law. In the dislocation starvation model [15], the strength of the crystal is controlled by the inability of the dislocations initially present to multiply as they escape to the free surfaces. As both the dislocation content and the mean distance of dislocations to the free surface decrease with the size of the crystal, very small pillars tend to be starved more rapidly causing a strong hardening and thus explaining the size effect. The starvation process has been observed during in-situ Transmission Electron Microscopy (TEM) compression experiments performed on small pillars made by focus ion beam (FIB) technique [16]. In this experiment, the initial microstructure consists mainly of irradiation defects caused by FIB milling. Upon straining, the starvation of the pillar results of the expulsion of these defects to the free surfaces.

In the source controlled model, internal stable dislocation sources are able to operate, preventing the crystal from starvation [17], [18]. In this case the size effect arises from the increasing stress required to activate these sources in small crystals. Indeed, as shown in [17], the source strength increases statistically when they are more confined. Recent TEM experiments [19] [20] performed on thin films that were kept free from FIB defects show that the dislocation density in a small crystal strained in tension is kept constant during the deformation, indicating that dislocations can be nucleated at an appropriate rate before escaping. Similar observations were also obtained in FIB copper sub-micron pillars tested in compression [21]. However stable sources have not yet been reported.

In the present work, we show evidence of stable dislocation sources inside FIB-free sub-micron Al single crystals observed during in-situ tensile TEM experiments. This situation

author's personal copy

contrasts with the observation of intermittent plastic events and dislocation starvation in fibers were irradiation defects were introduced in purpose using FIB milling. These new results highlight the importance of the initial microstructure and the way small objects are prepared on plasticity.

Experimental

A lamellar Al/Al_2Cu eutectic alloy with a 2 µm average lamellae spacing was produced using a directionally solidification technique [22]. 2.5 x 1 x 0.5 mm rectangles were cut using spark machining and thinned down to 30µm using diamond polishing papers. The lamellae are oriented perpendicular to the flat surface of the rectangle and aligned along its largest dimension. Electropolishing of these thin rectangles using a solution of methanol with 33% of nitric acid at T=-10°C and I=500mA produced a concavity where the Al_2Cu lamellae are polished faster. Al fibers are also polished, but at a slower rate, resulting in a "comb" structure (**Figure 1**). Because of a longer etching time in the center of the dimple compared to its sides, thicker Al fibers are found near the edges of the concavity. With this procedure, the fabrication of one TEM sample results in a set of Al fibers with a similar crystalline orientation and different lengths and sections. The fiber section was measured either post-mortem or in-situ. In the post-mortem method, the fiber was cut by FIB in or near the plastically deformed area and the cross section was directly observed in SEM. In the in-situ method, sections are measured using both the glide plane inclination and the apparent glide plane section (i.e. the section of the glide plane projected in the observation plane). The sections were found to range from a few μm^2 down to 0.08μm^2, which correspond to thickness – or more generally to the smallest axis of an ellipse – d ranging from 0.1µm to 1.2µm. Two freestanding fibers are shown in **Figure 1b**. The thicker fiber A was carved out by FIB using a Ga^+ ion beam of 50 pA for about a minute in order to reduce its section. During this process, the fiber A, located on the left, was accidentally irradiated with the ion

author's personal copy

beam. Its microstructure and behaviour upon straining will be described below. Non-irradiated fibers located in other area of the specimen were also observed.

The rectangular sample was glued with cyanocrylate or epoxy to a copper grid that fits the straining holder, so that the fibers stand along the straining axis. In situ TEM experiments were carried out in strain control. Strain increments of 50-100 nm were applied to the Cu grid. Real strain increments are calculated through the number of dislocations shearing the fiber, when possible. Relaxation mechanisms were followed with a Megaview III camera (Soft Imaging System-Olympus) and recorded on a DVD/Hard drive video recorder at a rate of 25 images/s.

Results

Figures 2a and 2b show two dark field micrographs of the 325nm large 200nm thick irradiated fiber shown in **Figure 1b**. They were extracted from a video sequence taken during a straining experiment. The large number of small dislocations loops and segments is a direct consequence of irradiation damage due to the FIB [23], as those defects are not present in fibers produced by electropolishing (see below). Except for these defects, no long dislocations have been observed.

Upon straining, fast dislocation motions were observed. These movements occur within one frame (i.e. 0.04s) and lead to the formation of slip traces (noted Tr on **Figure 2b**) appearing as bright traces at the fiber surfaces. The corresponding slip plane is found to be the {111} plane with the most favourable orientation with respect to the tensile stress axis (T). Image difference of pictures taken before and after dislocation motion (**Figure 2c**) highlights the changes in the microstructure. Grey areas correspond to unchanged areas. Black and white contrasts indicate on the contrary that several dislocation defects were affected when the moving dislocation emerged at the free surface. After few tens of seconds the slip traces completely disappear indicating that the strain field of the emerging dislocation has faded out.

author's personal copy

Areas (see arrows in **Figure 2a**) where dislocations have glided contain however less irradiation defects indicating that some mechanical annealing has occurred, in agreement with the dislocation starvation model. Dislocation glide events occur repeatedly and no stable internal dislocation sources can be detected.

Figure 3 shows a fiber free of FIB defect with a similar width and thickness than the fiber shown in **Figure 2**. As expected, no irradiation defects are visible and the structure remains clear of any dislocations. Upon straining, the fiber suddenly fractured along a plane inclined approximately 45° from the tensile axis which corresponds to the plane with the highest resolved shear stress (**Figure 3b**). Although the stress cannot be determined during this experiment, this behaviour is typical of a whisker behaviour failing close to the theoretical stress, i.e. between $\mu/30$ and $\mu/2\pi$ [24], [25]. Despite similar size, FIB-irradiated and as-grown fibers exhibit clearly a distinct behaviour.

A ductile behaviour has been however observed in fibers containing initially at least few dislocations. **Figure 4** shows a 750nm large 180nm thick fiber containing an isolated dislocation source. It is composed of a fixed sessile arm (FA) around which a moving arm (MA) of Burgers vector ½[10-1] and located in the (111) plane turns as soon as sufficient stress is applied. In **Figure 4a**, the moving dislocation starts to bend under the stress because the line-tension force increases when the curvature increases. The transient equilibrium is reached when the dislocation curvature is minimum, i.e. when the distance L to the free surface is minimum. When the resolved shear stress τ exceeds a critical stress τ_{cr}, the curvature decreases and the dislocation expands and moves freely. This process repeats itself, resulting in an oscillatory stress cycle with a period matching that of the single-arm windmill motion, which appears jerky. The dislocation is eventually pinned near the surfaces where it leaves slip traces (**Figure 4b**). As observed in **Figure 2**, the traces disappear within few tens of seconds. The source continues to operate during several minutes. **Figure 4c** shows the formation of a transient pile-up after 3 dislocations have been emitted in a short period of time

author's personal copy

due to a slight increase of the strain rate. As the pile up forms, a back stress, which increases with the number of trapped dislocations, is exerted on the moving segment of the source. The applied resolved shear stress should then increase to counterbalance this back stress, causing thus hardening.

Figure 4d shows the image of the source projected in the (111) glide plane. Anisotropic calculation using the DISDI software [26] shows that the shape of the moving arm can be well fitted by an ellipse elongated along the screw direction. The strength of the source can then be estimated using line tension calculation and leads to a resolved shear stress $\tau \approx 230$MPa. The applied stress can be retrieved using the Schmid relation. In this case, the Schmid factor is 0.46, which yields to $\sigma \approx 500$ MPa. Since this calculation is only valid for an isolated dislocation loop, the shape of the loop is not well described when close to the fixed arm and close to the surface, where image force and elastic interaction with the fixed arm operate respectively.

The strength of several sources have been determined and are plotted in **Figure 5** (red square) as a function of the inverse characteristic length d (see the Experimental section). Blue points have been obtained by instrumented in-situ SEM tests as reported in a previous study [27]. Systematic error bars on the in-situ TEM points arise from the uncertainty in determining both the ellipse shape at the critical configuration of the moving arm and the fiber thickness. Despite some scatter in the results, **Figure 5** shows a good agreement between mechanical tests and in-situ measurements, establishing that the yield stress is directly caused by the operation of spiral sources. The data points can be fitted by the relation $\sigma = \frac{k}{d}$ with k a constant, that is with an exponent n=1 (see Introduction). For the smallest fiber, the yield stress approaches 1.3GPa which is of the order of the lower theoretical stress ($\mu/2\pi$=4.1GPa, $\mu/30$=0.9GPa).

author's personal copy

The variation of the yield stress can be discussed in term of source strength. Indeed, the source strength depends on first approximation linearly to the inverse of the curvature of the moving arm at the critical position. This curvature is set by the distance between the fixed arm and the free surface. As the average distance of a source to the free surface decreases, the source strength is expected to increase linearly with the fiber characteristic size. An exponent of 1 in the power law is also consistent with recent Discrete Dislocation Dynamics simulations that reproduce a real initial microstructure with intermittent sources [28]. However, because of the statistical distribution of the sources in the fiber, the yield stress will show some variation depending on the number of available sources [17]. Larger deviations from this law are thus expected for low density fibers. This conclusion is in agreement with the variation of the power law exponent in the literature.

The slight differences in the slope between instrumented and in-situ TEM can have different origins. In particular the strain/relaxation rates are different with typically a value of $10^{-6}s^{-1}$ for in situ TEM experiments and $10^{-4}s^{-1}$ for SEM tests. The effect of the strain rate can be assessed directly during the operation of a spiral source. Indeed, a higher strain rate directly causes an increase of the source speed which induces the formation of a pile up against the native oxide at the surface, and thus a back stress on the source. Because the dislocations probably escape by a diffusive process in the oxide layer similar to dislocation spreading observed in high angle grain boundary [29], the strain hardening coefficient is supposed to strongly increase if the characteristic time for dislocation escape is of the order or smaller than the source rate. Indeed, in this case the back stress due to the eventually formed pile up strongly increases preventing the source from operating. More, because the back stress is inversely proportional to the length of the pile-up, the strain hardening should increase for a given strain rate with a decreasing characteristic fiber length. This seems to be in agreement with recent results in copper [30].

author's personal copy

Conclusions

Aluminum sub-micron fibers have been strained in-situ in TEM. This type of experiments allows the observation of elementary plastic mechanisms at fiber scale and in real time. We have found that plastic deformation depend on the initial dislocation microstructure. Intermittent plastic events and dislocation escape have been observed when the initial microstructure is composed by a high density of irradiation defects due to FIB preparation. On the contrary, when these defects are suppressed, and fiber left free from dislocation, the fiber deform by fracture like whiskers. When dislocations are initially present, we found that stable single source can carry plasticity in a very smooth manner. The increase of the yield stress with decreasing fiber characteristic length can be directly attributed to the increase of the strength of these sources.

Received: ((will be filled in by the editorial staff))
Revised: ((will be filled in by the editorial staff))
Published online: ((will be filled in by the editorial staff))

[1] J. R. Greer and J. T. M. De Hosson, *Progress in Materials Science* **2011**, *56*, 654-724.
[2] O. Kraft, P. A. Gruber, R. Mönig and D. Weygand, *Annual Reviews of Materials Research* **2010**, *40*, 296-317.
[3] S. S. Brenner, *Journal of Applied Physics* **1957**, *28*, 1023–1026.
[4] G. Richter, K. Hillerich, D. Gianola, R. Mönig, O. Kraft and C. Volkert, *Nano Letters* **2009**, *9*, 3048-3052.
[5] M. D. Uchic, D. M. Dimiduk, J. N. Florando and W. D. Nix, *Science* **2004**, *305*, 986-989.
[6] D. M. Dimiduk, C. Woodward, R. LeSar and M. D. Uchic, *Science* **2006**, *312*, 1188-1190.
[7] C. A. Volkert and E. T. Lilleodden, *Philosophical Magazine* **2006**, *86*, 5567-5579.
[8] C. P. Frick, B. G. Clark, S. Orso, A. S. Schneider and E. Arzt, *Materials Science and Engineering: A* **2008**, *489*, 319-329.
[9] D. Kiener, C. Motz and G. Dehm, *Materials Science and Engineering: A* **2009**, *505*, 79-87.
[10] A. S. Schneider, D. Kaufmann, B. G. Clark, C. P. Frick, P. A. Gruber, R. Mönig, O. Kraft and E. Arzt, *Physical Review Letters* **2009**, *103*, 105501.
[11] H. Bei, S. Shim, M. K. Miller, G. M. Pharr and E. P. George, *Applied Physics Letters* **2007**, *91*, 111915.
[12] H. Bei, S. Shim, G. Pharr and E. George, *Acta Mater.* **2008**, *56*, 4762-4770.
[13] P. S. Phani, K. E. Johanns, G. Duscher, A. Gali, E. P. George and G. M. Pharr, *Acta Materialia* **2011**, *59*, 2172-2179.

author's personal copy

[14] H. Bei, S. Shim, E. George, M. Miller, E. Herbert and G. Pharr, *Scripta Mater.* **2007**, *57*, 397-400.
[15] J. R. Greer and W. D. Nix, *Physical Review B* **2006**, *73*, 245410 .
[16] Z. W. Shan, R. K. Mishra, S. A. S. Asif, O. L. Warren and A. M. Minor, *Nature Materials* **2008**, *7*, 115-119.
[17] T. A. Parthasarathy, S. I. Rao, D. M. Dimiduk, M. D. Uchic and D. R. Trinkle, *Scripta Materialia* **2007**, *56*, 313-316.
[18] K. S. Ng and A. H. W. Ngan, *Scripta Materialia* **2008**, *59*, 796-799.
[19] S. H. Oh, M. Legros, D. Kiener, P. Gruber and G. Dehm, *Acta Materialia* **2007**, *55*, 5558-5571.
[20] S. H. Oh, M. Legros, D. Kiener and G. Dehm, *Nature Materials* **2009**, *8*, 95-100.
[21] D. Kiener and A. Minor, *Nano Lett.* **2011**, *11(9)*, 3816–3820.
[22] J. Riquet and J. Durand, *Journal of Crystal Growth* **1975**, *29*, 217.
[23] D. Kiener, C. Motz, M. Rester, M. Jenko and G. Dehm, *Materials Science and Engineering: A* **2007**, *459*, 262-272.
[24] S. Ogata, J. Li and S. Yip, *Science* **2002**, *298*, 807-811.
[25] A. T. Paxton, P. Gumbsch and M. Methfessel, *Philosophical Magazine Letters* **1991**, *63*, 267 - 274.
[26] J. Douin, P. Veyssière and P. Beauchamp, *Phil. Mag.* **1986**, *54*, 375–393.
[27] F. Mompiou, M. Legros, A. Sedlmayr, D. Gianola, D. Caillard and O. Kraft, *Acta Materialia*.
[28] C. Motz, D. Weygand, J. Senger and P. Gumbsch, *Acta Materialia* **2009**, *57*, 1744-1754.
[29] J. Kwiecinski and J. Wyrzykowski, *Acta metall. mater.* **1991**, *39(8)*, 1953–1958.
[30] D. Kiener, P. J. Guruprasad, S. M. Keralavarma, G. Dehm and A. A. Benzerga, *Acta Materialia* **2011**, *59*, 3825-3840.

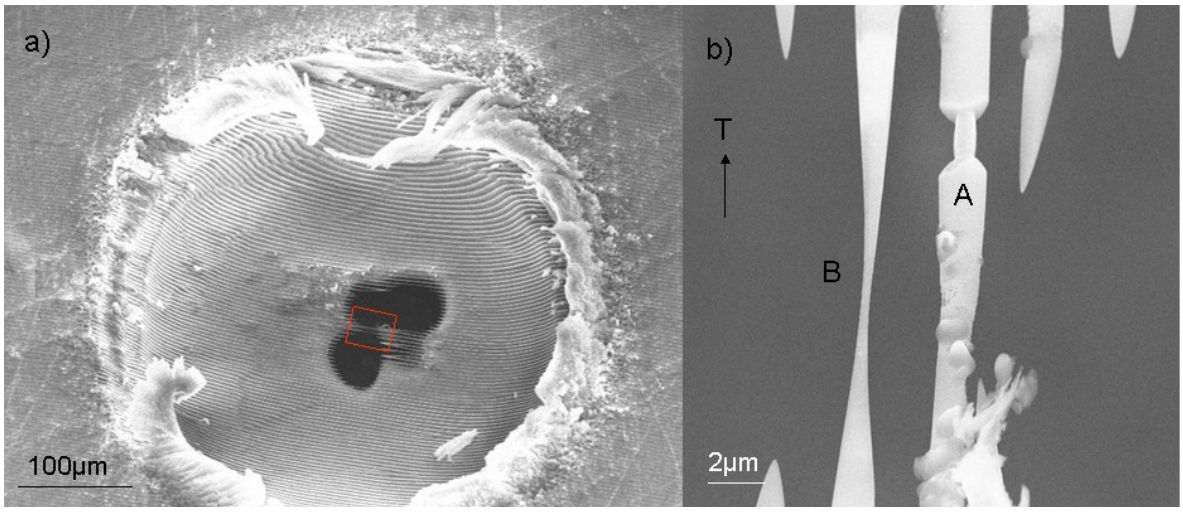

Fig. 1. a) A TEM sample obtained after etching a directionally solidified Al/Al_2Cu lamellar eutectic alloy. Because the etching is faster for the Al_2Cu phase than for Al, electron transparent Al fibers are obtained in the center hole. b) Zoom of the central area indicated in a). All the fibers were strained at the same time along their longest direction (T). The thick fiber A was carved by FIB in order to reduce their sections. During this process, the fiber B was also irradiated by Ga ion.

author's personal copy

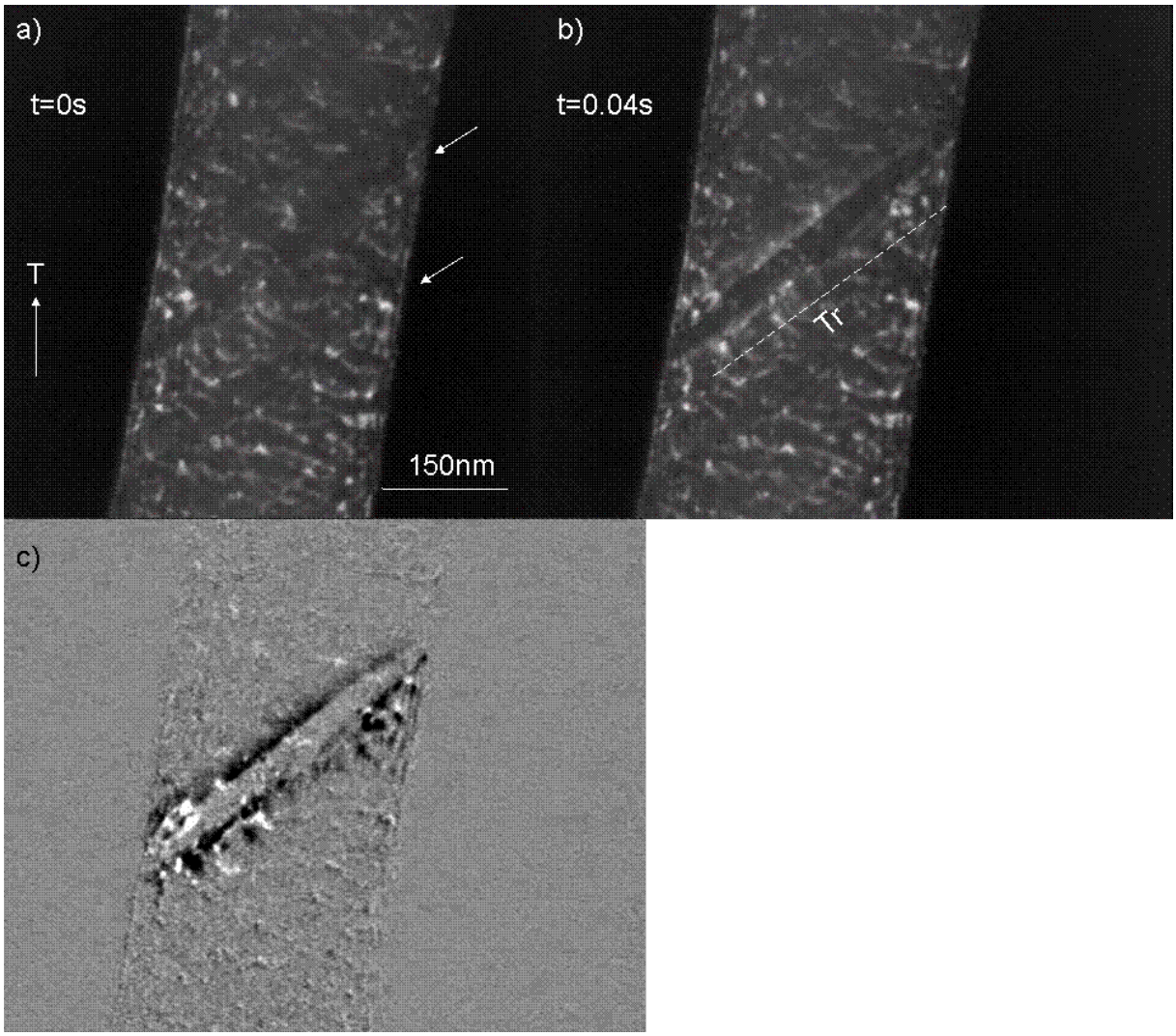

Fig. 2. Dark fields micrographs of a fibers exposed to Ga^+ ions and strained along the direction T. The high density of small dislocations near the surface is caused by ion irradiation. A fast dislocation motion occurred in b) along a slip plane which intersects the surface along the direction Tr (slip traces). c) Image difference b)-a) showing dislocation activity near slip traces. Channels marked by arrows in a) are evidence of dislocation clearing caused by dislocation glide.

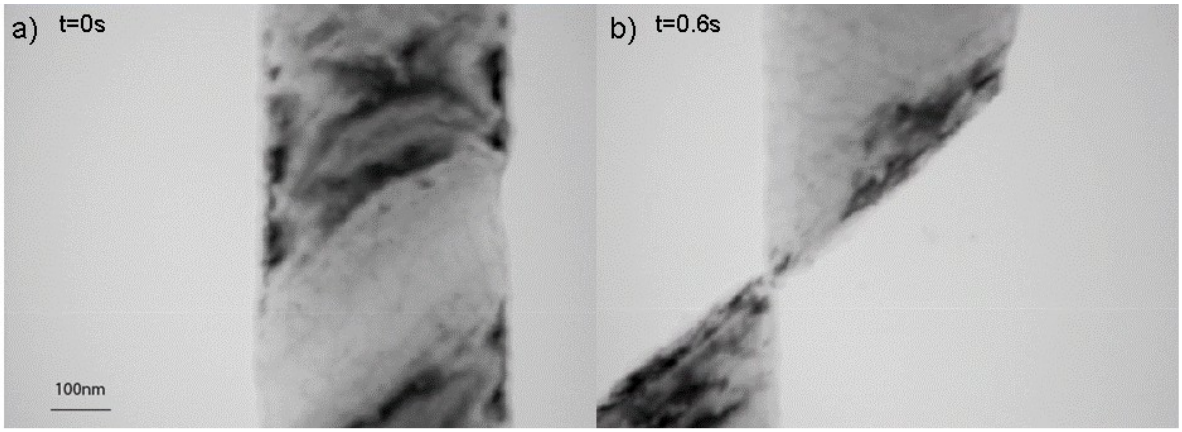

Fig. 3. Bright field images extracted from a video sequence taken during an in-situ straining experiment and showing brittle fracture in a defect free fiber.

author's personal copy

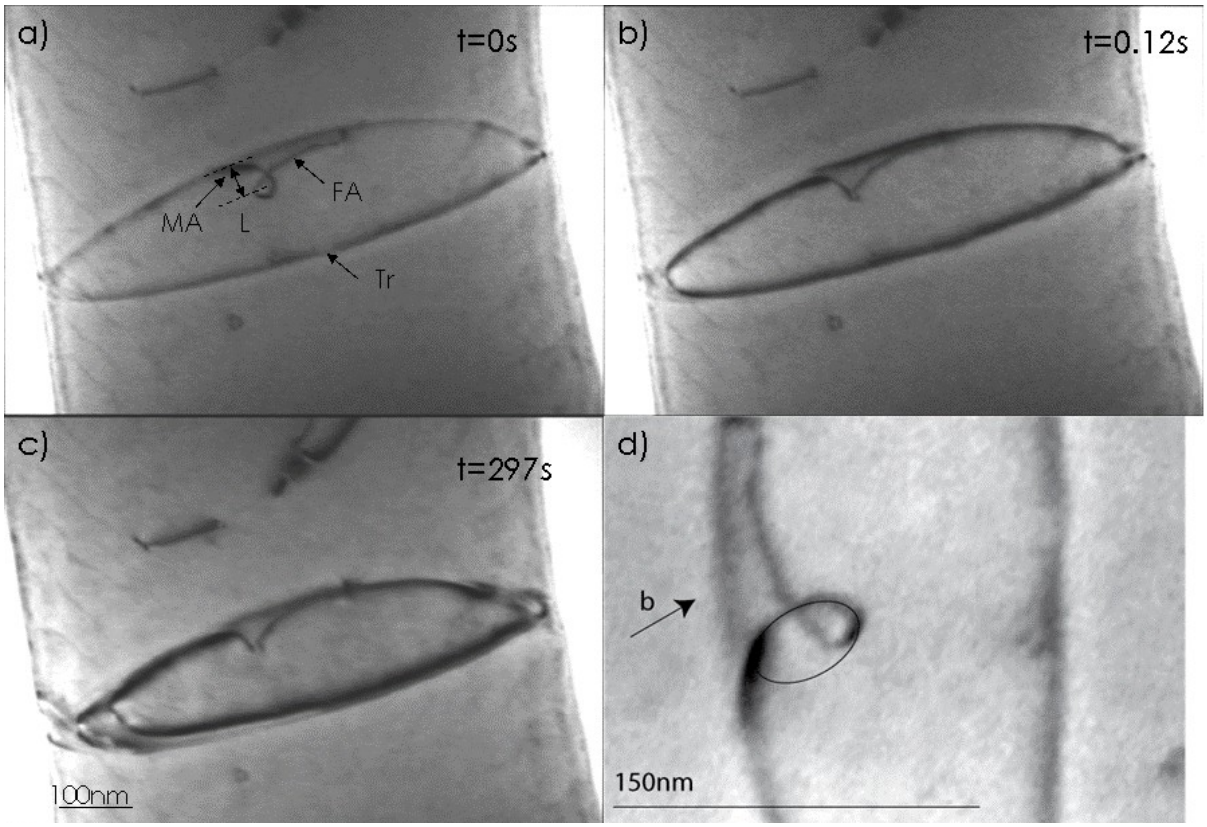

Fig. 4. Single spiral source operating in a FIB defect free fiber. The source is composed of a fixed arm (FA) around which a moving arm (MA) turns. Every turn, a new dislocation of Burgers vector 1/2[10-1] gliding in the (111) plane intersects the free surface leaving a slip trace (Tr). c) A pile-up can form transitorily below the surface in front of the oxide layer. d) The dislocation shape projected in its glide plane can be well fitted by an ellipse according to line tension calculation.

author's personal copy

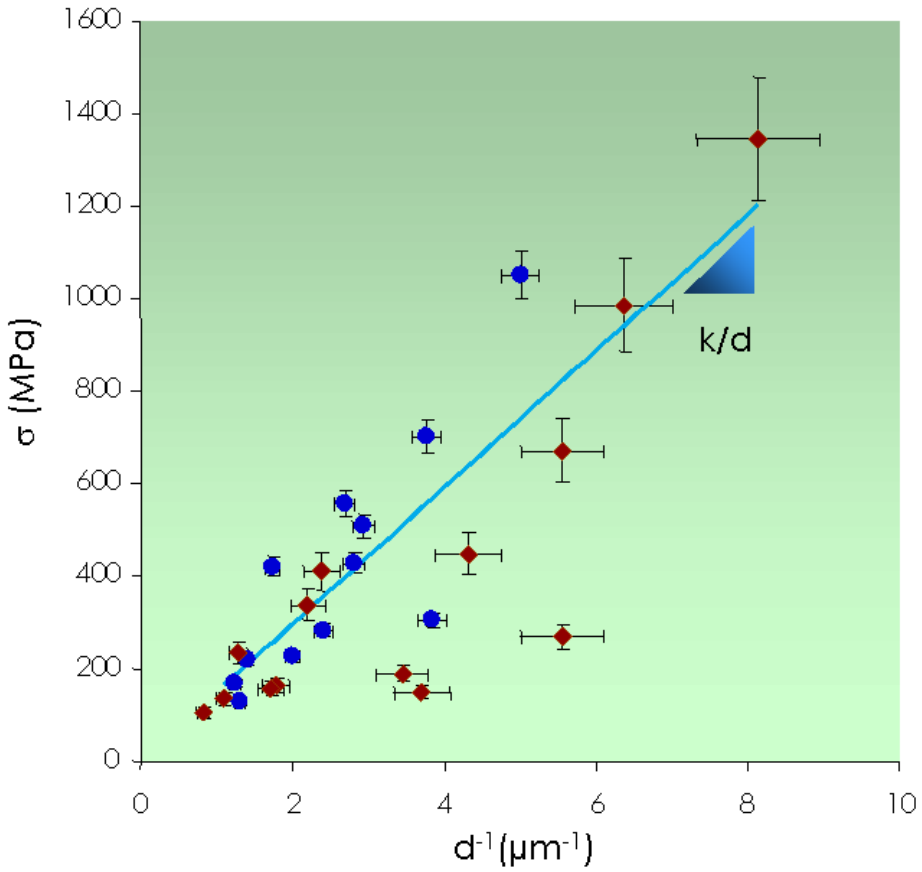

Fig. 5. Yield stress of individual fibers as a function of the inverse fiber characteristic length d. Red diamond points correspond to in-situ TEM measurements and round blue points to instrumented SEM tests.